Journal of Materials Science: Materials in Medicine (2020) 31:43
https://doi.org/10.1007/s10856-020-06378-6

TISSUE ENGINEERING CONSTRUCTS AND CELL SUBSTRATES

Original Research

Electrophoretic processing of chitosan based composite scaffolds with Nb-doped bioactive glass for bone tissue regeneration

Lorenzo Bonetti[1] · Lina Altomare[1,2] · Nina Bono[1] · Eliana Panno[1] · Chiara Emma Campiglio[1] · Lorenza Draghi[1,2] · Gabriele Candiani[1,2] · Silvia Farè[1,2] · Aldo R. Boccaccini[3] · Luigi De Nardo[1,2]

Received: 24 October 2019 / Accepted: 5 April 2020 / Published online: 1 May 2020

Abstract

Bioactive glasses (BGs), due to their ability to influence osteogenic cell functions, have become attractive materials to improve loaded and unloaded bone regeneration. BG systems can be easily doped with several metallic ions (e.g., Ag, Sr, Cu, Nb) in order to confer antibacterial properties. In particular, Nb, when compared with other metal ions, has been reported to be less cytotoxic and possess the ability to enhance mineralization process in human osteoblast populations. In this study, we co-deposited, through one-pot electrophoretic deposition (EPD), chitosan (CS), gelatin (GE) and a modified BG containing Nb to obtain substrates with antibacterial activity for unloaded bone regeneration. Self-standing composite scaffolds, with a defined porosity (15–90 μm) and homogeneous dispersion of BGs were obtained. TGA analysis revealed a BG loading of about 10% in the obtained scaffolds. The apatite formation ability of the scaffolds was evaluated in vitro in simulated body fluid (SBF). SEM observations, XRD and FT-IR spectra showed a slow (21–28 days) yet effective nucleation of CaP species on BGs. In particular, FT-IR peak around 603 cm^{-1} and XRD peak at $2\theta = 32°$, denoted the formation of a mineral phase after SBF immersion. In vitro biological investigation revealed that the release of Nb from composite scaffolds had no cytotoxic effects. Interestingly, BG-doped Nb scaffolds displayed antibacterial properties, reducing *S. lutea* and *E. coli* growth of ≈60% and ≈50%, respectively. Altogether, the obtained results disclose the produced composite scaffolds as promising materials with inherent antibacterial activity for bone tissue engineering applications.

Graphical Abstract

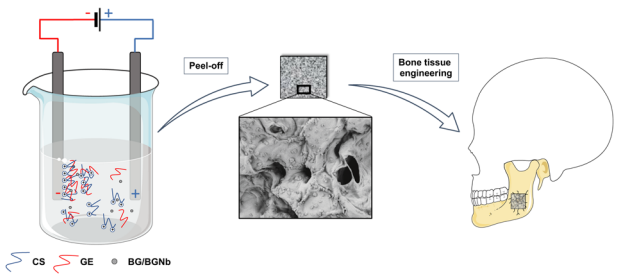

1 Introduction

Composite scaffolds designed for hard tissue regeneration are usually made of a polymeric matrix embedding inorganic materials in order to reproduce the typical structure of

Supplementary information The online version of this article (https://doi.org/10.1007/s10856-020-06378-6) contains supplementary material, which is available to authorized users.

✉ Lina Altomare
lina.altomare@polimi.it

[1] Department of Chemistry, Materials and Chemical Engineering "G. Natta", Politecnico di Milano, Piazza Leonardo da Vinci 32, 20133 Milan, Italy

[2] National Interuniversity Consortium of Materials Science and Technology (INSTM), 50121 Florence, Italy

[3] Institute of Biomaterials, University of Erlangen-Nuremberg, Cauerstrasse 6, 91058 Erlangen, Germany

bone, consisting of an organic phase (mainly collagen) and a mineral phase (mainly hydroxyapatite). The use of bioactive materials to mimic the inorganic component has emerged as promising approach to improve bone tissue regeneration [1]. In particular, bioactive glasses (BGs), with their ability to enhance bone tissue repair mechanisms and influence cell behavior through their dissolution [2], have become attractive platforms for improving the regeneration of loaded and unloaded bone [3].

Currently, novel formulations of BGs are under investigation showing that the biologically active release of different ions (i.e., silicon, calcium, phosphorus, magnesium and cobalt) from BG-loaded scaffolds can influence osteogenic cell functions, such as proliferation, differentiation and mineralization [4]. BG systems can be further modified via their doping with several metal ions, such as silver (Ag), strontium (Sr), copper (Cu), in order to enhance their antibacterial properties and angiogenesis [5, 6]. In particular, niobium (Nb), if compared with other metal ions, has been reported to induce lower cytotoxicity and has the ability to enhance mineralization process in human osteoblast populations [7, 8]. However, to the best of our knowledge, The potential antimicrobial activity of Nb has not been yet investigated.

The incorporation of active BGs into polymer matrices has been found to improve the osseointegration and mimic the biological processes leading to tissue regeneration. Natural polymers have gained attention due to their superior biocompatibility, biodegradability and their structural similarities with extracellular matrix (ECM) components [9]. Among the possible polymers, chitosan possesses interesting characteristics for bone tissue engineering (BTE), being a cationic, biodegradable natural polymer easily available at low costs. Specifically, chitosan has been shown to provoke an extremely reduced foreign body reaction, possesses an intrinsic antibacterial nature, and allows the incorporation and delivery of biologically active molecules [10, 11]. Moreover, it can be easily processed by electrophoretic deposition technique (EPD) that under the presence of an electric field allows the motion and deposition of charged chitosan molecules on metallic substrates [12]. Due to its versatility as a fabrication technique, EPD leads to the production of different substrates, including coatings for orthopedic implants [13, 14] and regularly shaped micropatterned scaffolds for bone tissue regeneration [15].

The addition of biomolecules, such as gelatin, in the polymer matrix during EPD may further enhance cell attachment and increase the biocompatibility of the scaffold [6]. Due to the presence of cell-interactive tripeptide sequences (RGD sequence) among gelatin polymer chains, the co-deposition of chitosan/gelatin matrix reinforced with BGs leads to the formation of a more suitable organic-inorganic substrate for the adhesion of osteoblast cells [16]. Moreover, EPD process allows the formation of micro-porous surfaces, that act as topographical cues for seeded cells, improving their initial attachment and differentiation [17]. In addition, such process induces the formation of a defined porous structure that can be tuned to elicit not only cell adhesion, but also the neovascularization of the implanted structure [15].

In this work, we aimed at demonstrating the suitability of organic-inorganic scaffolds, fabricated in a one-pot electrophoretic co-deposition procedure, as substrates with antibacterial activity for unloaded bone regeneration. In particular, by the co-deposition of chitosan, gelatin and a modified silicate BG containing Nb, we seek to minimize the risk of microbial contaminations taking advantage from coupling antibacterial effect of chitosan and niobium-doped BGs.

2 Materials and methods

2.1 Materials and chemicals

Chitosan (CS, 448877, 75–85% de-acetylated, medium molecular weight), acetic acid (AA, 320099), gelatin type B (GE, G9391), Phosphate-Buffered Saline (PBS) solution, salts (NaCl, $NaHCO_3$, KCl, K_2HPO_4 *$3H_2O$, $MgCl_2$ *$6H_2O$, HCl 1 M, $CaCl_2$, Na_2SO_4, and Tris) for Simulated Body Fluid (SBF) solution, were all provided by Sigma Aldrich (Milan, Italy) and used without purification. Niobium doped BG (BGNb, $D_{50} \sim 4$ µm) µm powder was prepared and characterized as reported elsewhere [18]. Bioactive glass of composition 45S5 (SCHOTT Vitryxx®, $D_{50} \sim 4$ µm) was used for comparison purposes.

2.2 Preparation of electrophoretic baths

CS (5 g L^{-1}) was dissolved in a 1% (w/w) AA solution in deionized water (dH_2O) at room temperature. The pH of the solution was set to 3.4 by dropwise addition of additional AA. The solution was then heated to 60 °C prior to the addition of GE (5 g L^{-1}) on a heating stirring plate (1.5 h, 600 rpm). CS-GE-BG and CS-GE-BGNb solutions were obtained by adding 10% (w_{BG}/w_{CS+GE}) BG powder or BGNb powder on the total polymer weight, respectively.

2.3 Scaffolds production

Deposition baths were degassed for 20 min with a nitrogen diffuser system and independently used as the electrolyte in a cell composed by a double-faced 20 × 20 mm^2 titanium (c.p., grade 2) cathode and two graphite rod anodes. EPD was performed using a 100 W power supply (Keithley 2425, Keithley Instruments), set in potentiostatic mode, applying a square waveform ($V_H = 50$ V, $V_L = 30$ V, duty cycle D = 0.5) for a deposition time of 5 min. The obtained scaffolds (namely CS-GE, CS-GE-BG, CS-GE-BGNb) were immersed

in dH_2O, peeled-off from the cathodes, and lastly freeze-dried for 24 h (Freeze drier Lio 5Pascal T = −40 °C, $p \leq 0.5$ mbar). Before the characterization, each sample was cut in 10 × 10 mm^2 specimens.

2.4 Morphological and thermogravimetric characterization

Analyses of the surface morphology of CS-GE-based scaffolds were performed with a Scanning Electron Microscope (Auriga CrossBeam, Carl Zeiss Microscopy). Briefly, samples were gold-sputtered, mounted onto scanning electron microscopy (SEM) stubs and examined using an acceleration voltage of 1 kV. SEM images were acquired at ×150, ×500 and ×1000 magnification. SEM images were subsequently processed (ImageJ, NIH, National Institutes of Health, USA) to quantify the micro-porosity of the scaffolds.

Thermogravimetric analyses (TGA, PerkinElmer SDA 6000) were performed to quantify the content of BG embedded in the CS-GE matrices. The mass variation, consequence of the thermal decomposition of the samples, was monitored between 35 and 900 °C, with a heating rate of 20 °C min^{-1} in air [15].

2.5 Swelling, degradation, and pH variation tests

The swelling properties of the scaffolds were studied in Phosphate-Buffered Saline solution (PBS, pH = 7.4, T = 37 °C) up to 28 days. The pH variations were monitored with a portable pH/ORP Meter (Hach HQ11d, Hach Company) at selected time-points, together with samples' weight variations. The swelling ratio (SW) of the samples was calculated according to Eq. (1):

$$\mathrm{SW}(\%) = \frac{\mathrm{w_t} - \mathrm{w_0}}{\mathrm{w_0}} \times 100, \quad (1)$$

where w_t (hydrated conditions) and w_0 (dry conditions) are the weights of the samples at time t and 0, respectively.

Degradation tests were performed on the samples maintained in PBS (T = 37 °C), and monitoring their weight at selected time-points up to 28 days. The degradation ratio (DR) of the samples was calculated according to Eq. (2):

$$\mathrm{DR}(\%) = \left[1 - \frac{\mathrm{w_p} - \mathrm{w_t}}{\mathrm{w_p}}\right] \times 100, \quad (2)$$

where w_p and w_t are the weights of the samples at swelling plateau (t = 5 h) and at time t, respectively.

2.6 Bioactivity evaluation

The scaffolds' bioactivity was evaluated in SBF solution. SBF was prepared (Supplementary Information 1) in accordance to ISO standard (ISO/FDIS 23317, "*Implants for surgery—In vivo evaluation for apatite-forming ability of implant materials*").

The samples were incubated in 6 mL of SBF (pH = 7.4), at 37 °C, under tangential agitation, up to 28 days. SBF was renewed every 3 days. At selected time-points, the samples were retrieved from SBF, rinsed with distilled water and freeze-dried [15].

Morphological features of the samples after SBF conditioning, at different time points, were evaluated by SEM analyses.

Both the chemical composition of the scaffolds and the possible formation of hydroxyapatite after in vitro bioactivity test were assessed by Fourier Transform Infrared Spectroscopy (FTIR, Shimadzu IRAffinity-1S). Data were collected in absorbance mode and acquired in the wavelength range of 4000–400 cm^{-1} with a resolution of 4 cm^{-1}. FTIR spectra were processed by the OriginPro software (OriginLab Corporation, United States—Fig. S1, Supplementary Information 2). The Savitzky–Golay filter was used after baseline subtraction. FTIR spectra were successively normalized to their global maximum peak as internal standard, divided into two regions (800–1200 cm^{-1} and 1200–1800 cm^{-1}) each one fitted by Gaussian functions (Fig. S2, Supplementary Information 2). The assignment of the peaks was performed according to previous literature.

Microstructure was characterized by X-Ray Diffraction (XRD, Rigaku MiniFlex 600 HR), operating with a Cu-Kα radiation (λ = 1.542 Å) at 40 kV and 15 mA. For qualitative analysis, XRD patterns were considered in the range of 20° < 2θ < 80° at a scan speed of 4° min^{-1} and a step size of 0.02°, in continuous mode.

2.7 In vitro biological studies

2.7.1 Scaffold preparation

CS-GE, CS-GE-BG and CS-GE-BGNb scaffolds were disinfected by immersion in pure ethanol, exposed to UV irradiation (30 min/side), and air-dried under a biological hood before indirect cytotoxicity and indirect antibacterial activity tests.

For biological tests (indirect cytotoxicity and antibacterial tests), sample extracts were prepared according to the ISO standard (ISO 10993–12:2012, "*Biological evaluation of medical devices—Part 12: Sample preparation and reference materials*"). Briefly, material extracts were obtained by placing sterile samples (n = 6) of each experimental group in separated 50 mL falcon tubes, in contact with the extraction vehicle (1 mL/100 mg of sample). Samples were next incubated at 37 °C for different time periods (8, 24, 28 h). At each time step, material extracts (eluates) were harvested and stored at −80 °C until use.

2.7.2 Indirect cytotoxicity test

Indirect cytotoxicity tests were performed according to the ISO standard (ISO 10993–5:2009, "*Biological evaluation of medical devices—Part 5: Tests for in vitro cytotoxicity*"). Standard cell culture medium (Dulbecco's Modified Eagle Medium (DMEM) containing 1 mM sodium pyruvate, 10 mM HEPES buffer, 100 U mL^{-1} penicillin, 0.1 mg mL^{-1} streptomycin, 2 mM glutamine and supplemented with 10% (v/v) fetal bovine serum (FBS), hereafter referred to as complete DMEM) was used as the extraction vehicle.

MG63 cells (human osteosarcoma cell line cells; American Type Culture Collection, ATCC, Manassas, VA, USA) were seeded in 96-well culture plates at a density of 10^4 cells/well in 100 µL of complete DMEM, and incubated in standard culture conditions (37 °C in a humidified atmosphere under constant supply of 5% CO_2) for 24 h. Afterwards, the medium was replaced with 50 µL/well of fresh medium and 50 µL/well of eluates (n = 3 wells/material sample/time point). Cells were next incubated for further 24 h in standard culture conditions. Cells cultured in complete DMEM were used as negative controls of cytotoxicity ($CTRL^-$, n = 3), while cells cultured in 0.5% phenol-containing complete DMEM were the positive controls of cytotoxicity ($CTRL^+$, n = 3). 24 h post-incubation, cell viability was assessed using resazurin assay (Sigma Aldrich). Briefly, the culture medium was discarded and each well was filled with 100 µL of specific medium containing 10 µL of resazurin dye solution. Cells were incubated in standard culture conditions for 2 h and the fluorescence (λ_{ex} = 540 nm; λ_{em} = 595 nm) of the supernatants was read by means of a GENios Plus reader (Tecan, Monza, Italy). Viability of $CTRL^-$ cells was assigned as 100%. For each well, cell viability was calculated according to the following Eq. (3):

$$\text{Viability}(\%) = \left[\frac{\text{RFU}_{\text{sample}}}{\text{RFU}_{\text{CTRL}^-}}\right] \times 100. \quad (3)$$

2.8 Indirect antibacterial test

Within indirect antibacterial tests, LB broth (Sigma Aldrich) served as the extraction vehicle.

Escherichia coli JM109 (*E. coli*, Gram negative bacteria, Leibniz Institute DSMZ, German Collection of Microorganisms and Cell Cultures, Braunschweig, Germany) and *Sarcina lutea* (*S. lutea*, Gram positive bacteria, ATCC 9341, ATCC) were pre-cultured overnight in 5 mL of LB broth at 37 °C under shaking at 130 rpm, until reaching an optical density (OD_{600nm}) of about 1, corresponding to ≈10^9 bacteria/mL. Bacterial suspensions were next diluted to a concentration of ≈10^6 bacteria/mL [19]. Afterwards, the bacterial suspension (50 µL/well) was passed into 96-well plates at a density of 1.5×10^5 bacteria cm^{-2} in 50 µL eluate/well (n = 3 wells/material sample/time point). Plates were next incubated at 37 °C for 24 h. Bacteria inoculated in 100 µL/well of LB were used as positive control for bacterial growth ($CTRL^+_{bacteria}$). The antibacterial efficacy of every eluate was evaluated by means of the turbidity method (i.e., OD_{600nm} measurements) [19]. Briefly, 24 h post-inoculum, the OD_{600nm} of each well (n = 3 per eluate) was read by means of a GENios Plus reader. The antibacterial efficiency was calculated according to the following Eq. (4):

$$\text{Antibacterial activity}\ (\%) = \left[1 - \frac{\text{OD}_{\text{sample}}}{\text{OD}_{\text{CTRL}^+_{\text{bacteria}}}}\right] \times 100. \quad (4)$$

2.9 Statistical analysis

Experiments were performed at least in triplicate (n = 3), and all data are expressed as mean ± standard deviation (SD). Statistical data analysis was carried out by GraphPad version 6 (GraphPad software, La Jolla, CA, USA). Comparisons among groups were performed by the one-way ANOVA. Significance was retained when $p < 0.05$.

3 Results

3.1 Morphological and thermogravimetric characterization

The morphology of the CS-GE-BG-based scaffolds obtained via EPD is reported in Fig. 1. In particular, a micro-porosity in the range of 20–130 µm can be observed for CS-GE scaffolds, and in the range of 15–90 µm for both CS-GE-BG and CS-GE-BGNb scaffolds. This means that micro-porosity roughly decreases in BG containing structures (Table 1). The distribution of BG and BGNb particles embedded in the CS matrix can be appreciated in Fig. 1c, f, i. The surface of CS-GE samples (Fig. 1c) appears smooth and no aggregates are shown. Instead, BG particles are present on both CS-GE-BG and CS-GE-BGNb samples (Fig. 1f, i, respectively), being distributed on their surface.

Interestingly, for both CS-GE-BG and CS-GE-BGNb samples, the diameter of the glass particles embedded in the scaffolds (Table 1) were comparable to the D_{50} value provided by Schott (D_{50}: 4 ± 1 µm). This suggests that the conditions selected for the EPD (e.g., bath composition, pH, electrical parameters) did not affect the morphology of the particles.

The presence of BG in the scaffolds was also confirmed by TGA analysis (Supplementary Information 3). By comparing the residual weight of the samples at 900 °C, a BG loading of 8.36 ± 0.10% and 10.28 ± 1.44% ($p > 0.05$, Table 1) has been obtained for CS-GE-BG and CS-GE-BGNb, respectively.

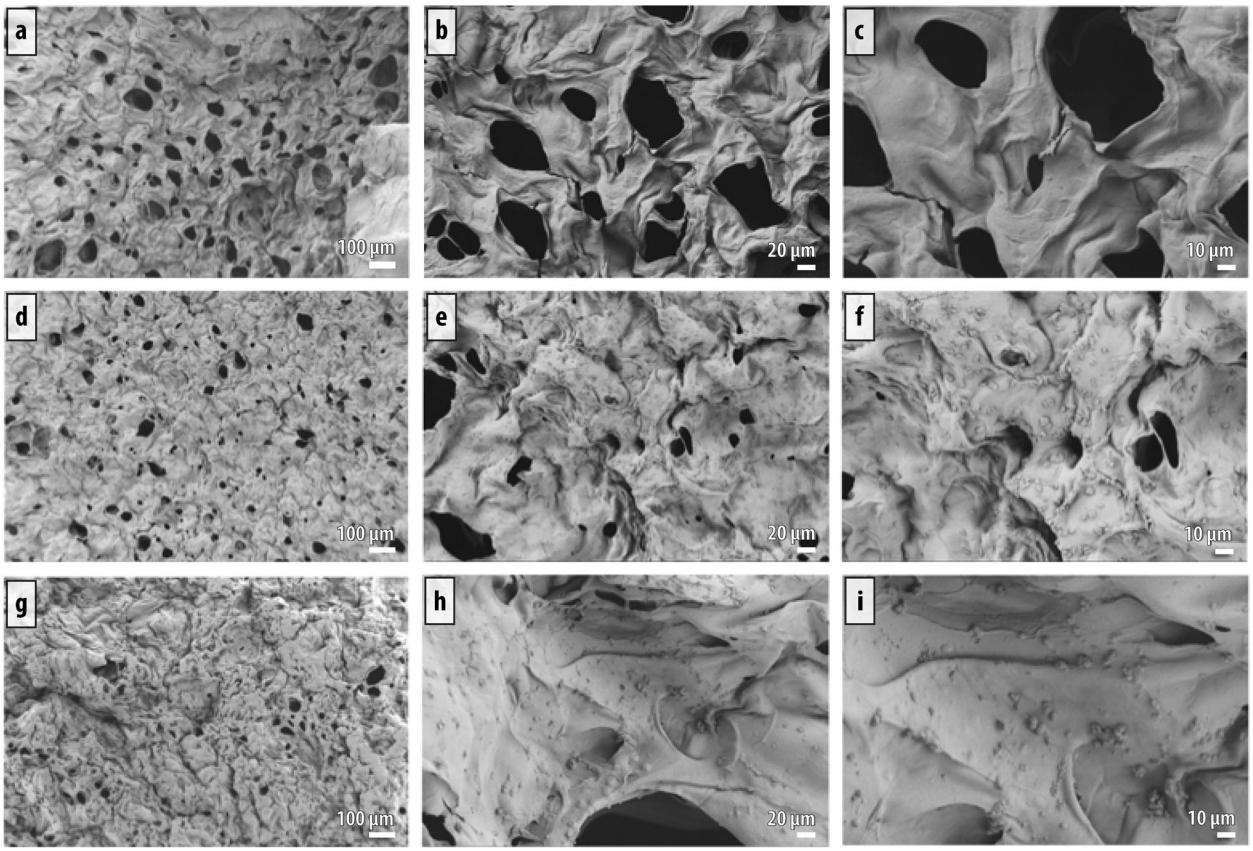

Fig. 1 SEM images of: CS-GE samples at **a–c** increasing magnification; CS-GE-BG samples at **d–f** increasing magnification; CS-GE-BGNb samples at **g–i** increasing magnification

Table 1 Pore diameters (micro-porosity) and glass content of the samples

Sample	Pore diameter [µm]	Glass particles diameter [µm]	Deposited glass [% w/w]
CS-GE	57.97 ± 28.12	–	–
CS-GE-BG	35.75 ± 15.96	3.20 ± 0.50	8.36 ± 0.10
CS-GE-BGNb	36.90 ± 16.81	3.71 ± 0.62	10.28 ± 1.44

The percentage of deposited glass was evaluated by TGA analysis

3.2 Swelling, degradation and pH variation tests

Figure 2 summarizes the swelling and degradation tests, and their effects on local pH, at the considered time-points up to 28 days. All samples swell immediately after immersion in PBS: specifically, CS-GE scaffolds show a significantly ($p < 0.05$) higher absorption capacity, reaching a maximum swelling rate of 817 ± 71%, compared to BG- and BGNb-containing samples (SR = 610 ± 58% and 550 ± 80%, respectively). For all the samples, the swelling plateau was reached after 120 min and no significant differences were found between the experimental groups (Fig. 2a).

Degradation tests in PBS for periods up to 28 days (Fig. 2b) highlight two different degradation kinetics, depending on the samples. After 28 days, CS-GE samples underwent a rapid degradation displaying a weight decrease of more than 70%, whereas CS-GE-BG and CS-GE-BGNb samples showed a slower degradation (weight decrease of about 45 and 40%, respectively) in the same timeframe. It is worthy of note that CS-GE-BG and CS-GE-BGNb profiles follow almost the same trend (Fig. 2a, b), thus showing that the incorporation of Nb resulted in a negligible influence in terms of swelling and degradation behavior.

Figure 2c shows the pH variations of PBS solution over time of immersion. After 5 h, a rapid increase of pH of the PBS solutions containing CS-GE, CS-GE-BG and CS-GE-BGNb samples can be observed, reaching an average pH of 7.84 ± 0.12, 7.89 ± 0.08 and 7.83 ± 0.08, respectively. No short-term (t < 5 h) significant differences were observed in the pH values between samples. pH values were also monitored up to 28 days (Fig. 2d). Apart from a rapid initial increase for all the considered samples, pH long-term variations are not significantly different, detecting pH values in the 7.74 and 7.92 range.

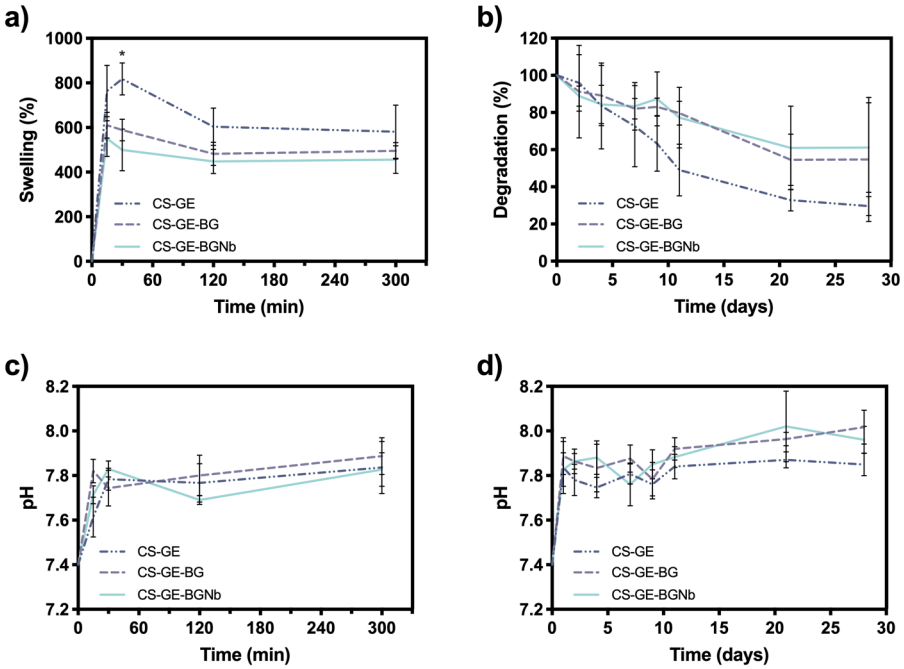

Fig. 2 Swelling rate (**a**), degradation rate (**b**), short-term (**c**) and long-term (**d**) pH variation of CS-GE, CS-GE-BG and CS-GE-BGNb samples. *$p < 0.05$ with respect to the other groups

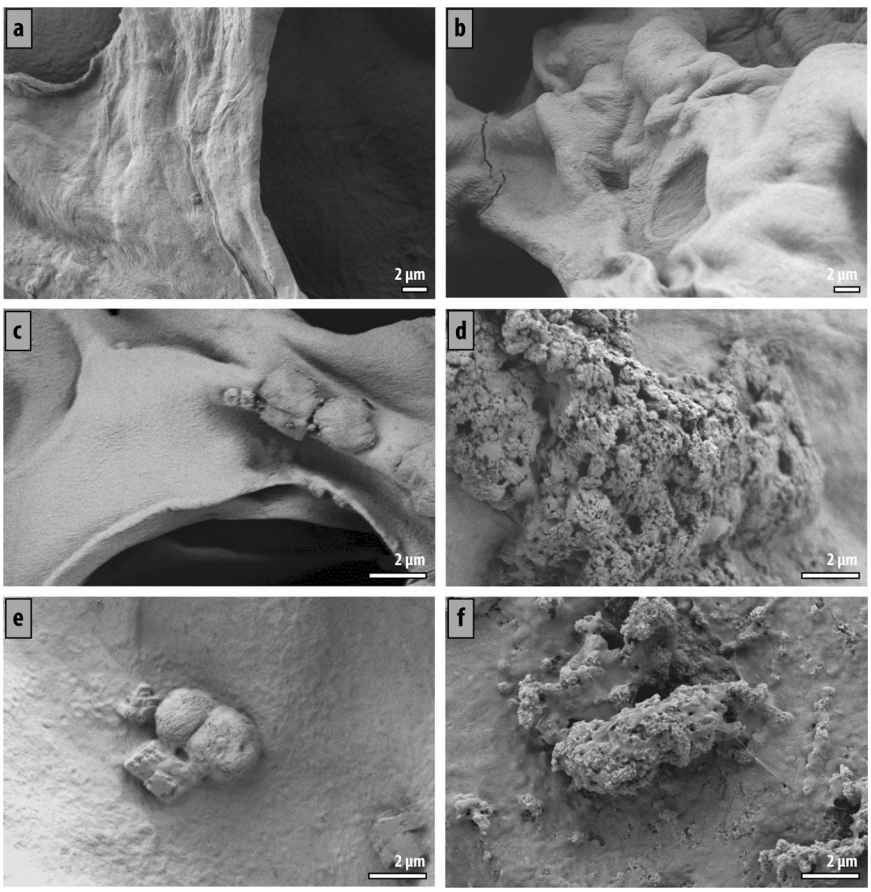

Fig. 3 SEM images of: CS-GE samples **a** before and **b** 28 days after SBF soaking; CS-GE-BG samples **c** before and **d** 28 days after SBF soaking; CS-GE-BGNb samples **e** before and **f** 28 days after SBF soaking. Scale bar = 2 µm

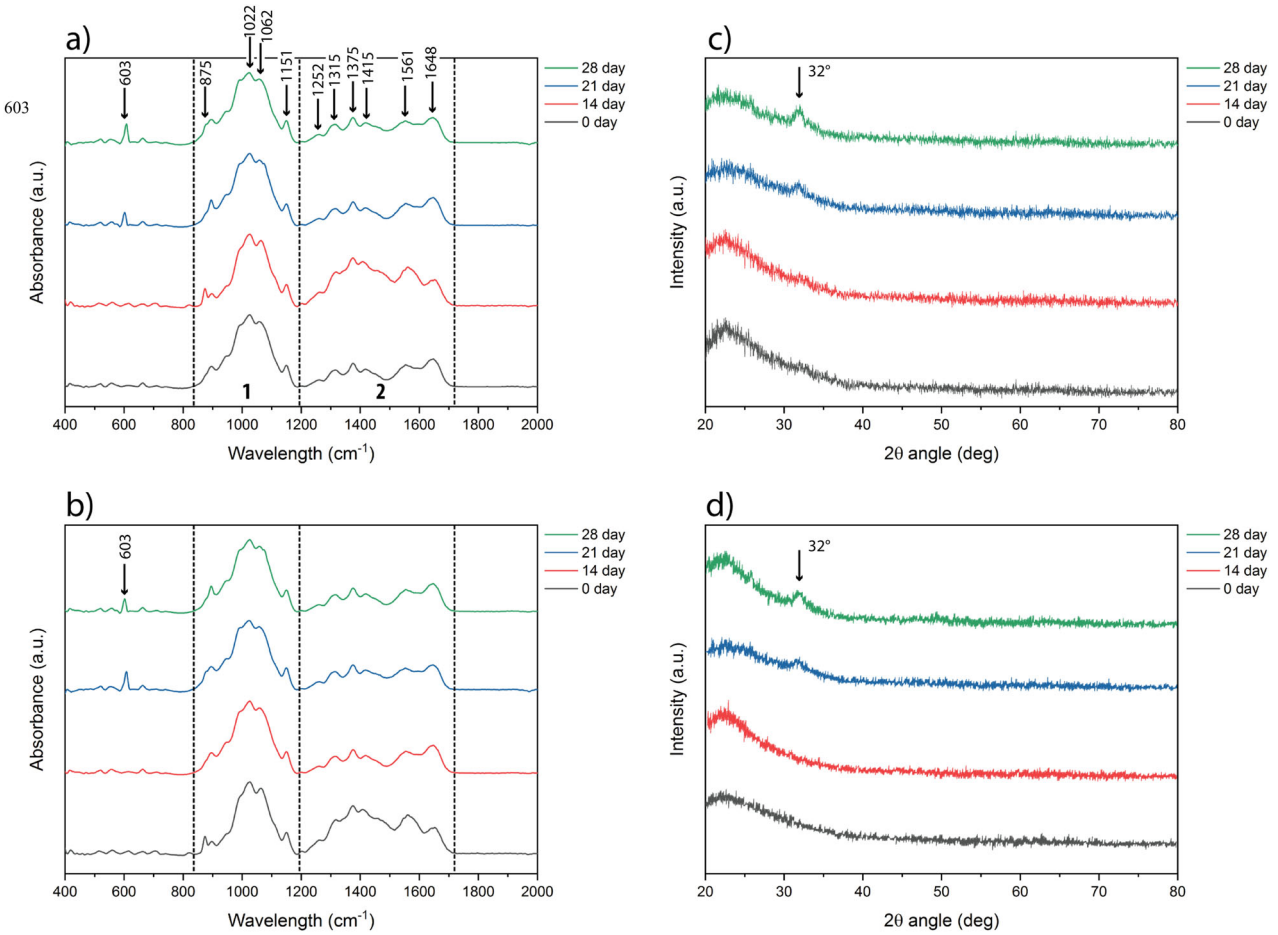

Fig. 4 FTIR spectra of **a** CS-GE-BG and **b** CS-GE-BGNb samples up to 28 days. XRD spectra of **c** CS-GE-BG and **d** CS-GE-BGNb samples up to 28 days. Two regions, delimited by dotted lines, were identified for spectral deconvolution

3.3 Bioactivity evaluation

Figure 3 shows the surface morphology of the samples before and after 28 days of soaking in SBF, obtained by SEM observations.

No morphological differences were found before and after soaking in SBF in CS-GE samples (Fig. 3a, b) that appear smooth and free of deposits. SEM images of CS-GE-BG samples (Fig. 3c, d) show the presence of uniform and smooth glass particles on the scaffold at day 0 (Fig. 3c). At day 28 (Fig. 3d), wide inhomogeneous aggregates appear on the samples surface, covering almost completely the glass particles. Similar observations can be done for CS-GE-BGNb samples (Fig. 3e, f).

FTIR spectroscopy was exploited to evaluate the interactions between polymers (GE and CS) and particles (BG and BGNb), and the formation of a HA layer on the surface of BG after immersion in SBF. FTIR spectra of CS-GE-BG and CS-GE-BGNb samples are shown in Fig. 4a, b, respectively. According to the literature, the presence of GE was confirmed by a defined peak, around 1648 cm^{-1} (1630 cm^{-1} [6]), attributed to the N-H stretching vibration of Amide I, and by the peak at 1252 cm^{-1} (1263 cm^{-1} [6]) associated to the stretching vibrations of -NH and -CH groups of Amide III. The presence of CS was confirmed by the peaks around 1022 cm^{-1} and 1062 cm^{-1}, attributed to the O-H bending and C-O stretching in chitosan, respectively [6]. Residual N-acetyl groups on chitosan were confirmed by the peak at 1315 cm^{-1} (1325 cm^{-1} [20]), attributed to C-N stretching of Amide III. Two bands at 1375 cm^{-1} and 1415 cm^{-1} (1423 cm^{-1} [20]) confirmed the presence of CH_3 symmetrical deformation and CH_2 bending on chitosan, respectively [20]. Moreover, the incorporation of CS in GE shifted the peak at 1165 cm^{-1}, relative to the stretching vibration of carboxyl (-COOH) groups of Glu and Asp in gelatin [21], to 1151 cm^{-1}.

Two absorption bands typical of the BG should be observed at 1010 cm^{-1} and 1060 cm^{-1}, corresponding to the asymmetric stretching vibration of Si-O-Si bonds [22]. However, both of them are superimposed to the peaks related to O-H bending (1022 cm^{-1}) and C-O stretching (1062 cm^{-1}) in chitosan. Thus, the presence of BG in

CS-GE-BG and CS-GE-BGNb samples was mainly confirmed by the peak in the range of 860–920 cm^{-1}, related to the Si-O-Si symmetric stretch of non-bringing oxygen atoms [23]. According to the literature [24], a band at 910 cm^{-1} indicates Nb-O bond vibration in the NbO_6 octahedral units. However, the presence of Si-O-Si symmetric stretch (860–920 cm^{-1}) partially superimposes. FT-IR peaks around 603 cm^{-1}, ascribable to P-O bending vibration [25], indicates the formation of a layer of calcium phosphates ($CaO\text{-}P_2O_5$) on CS-GE-BG and CS-GE-BGNb samples starting from day 21 (Fig. 4a, b). The formation of hydroxycarbonate apatite (HCAp) is usually confirmed by the characteristic peaks at 875 and 1420 cm^{-1} [26]. However, the absorption band at 1420 cm^{-1} was partially superimposed to the absorption bands of chitosan. In our work, the occurrence of carbonate peak at 875 cm^{-1} was used as evidence of HACp formation in the scaffolds.

XRD analyses were performed on all the samples in order to assess the presence of apatite crystalline phases on the glass surfaces after immersion in SBF. XRD spectra of the samples before and after soaking in SBF are shown in Fig. 4c, d. A wide peak at $2\theta = 22°$, presents in all XRD spectra, is ascribable to the amorphous CS matrix phase. Figure 4c shows no peak for CS-GE-BG samples soaked in SBF up to 14 days. A small peak at $2\theta = 32°$ appears after 21 and 28 days of immersion for CS-GE-BG and CS-GE-BGNb (Fig. 4c, d). According to the JCPDS (no. 09–0432) standard, this peak is usually assigned to apatite [27].

3.4 Biological tests

Indirect cytotoxicity tests, performed by challenging MG63 cells with material extracts for different time periods, were preliminarily performed in order to evaluate the cytotoxic effects of the material itself. Results reported in Fig. 5a show that the viability of cells incubated with material extracts (eluates) was comparable to those of cells cultured under standard conditions ($p > 0.05$ for all the conditions tested). Interestingly, these results demonstrate that CS-GE-BGNb scaffolds displayed a release of Nb ions at a concentration far from being cytotoxic, so that cell viability was totally unaffected.

Since the development of biomaterials with antimicrobial properties to prevent implant-associated infection is of paramount importance in the BTE field, in this study we also evaluate the antibacterial activity of CS-GE-BG-based scaffolds. The antibacterial activity of such materials was tested against *E. coli* and *S. lutea* bacteria as model organisms for Gram-negative and Gram-positive bacterial strains, respectively. More specifically, such bacteria are part of the human flora (*E. coli* are found in gut microbiota, while *S. lutea* may be found in the skin and large intestine) [19].

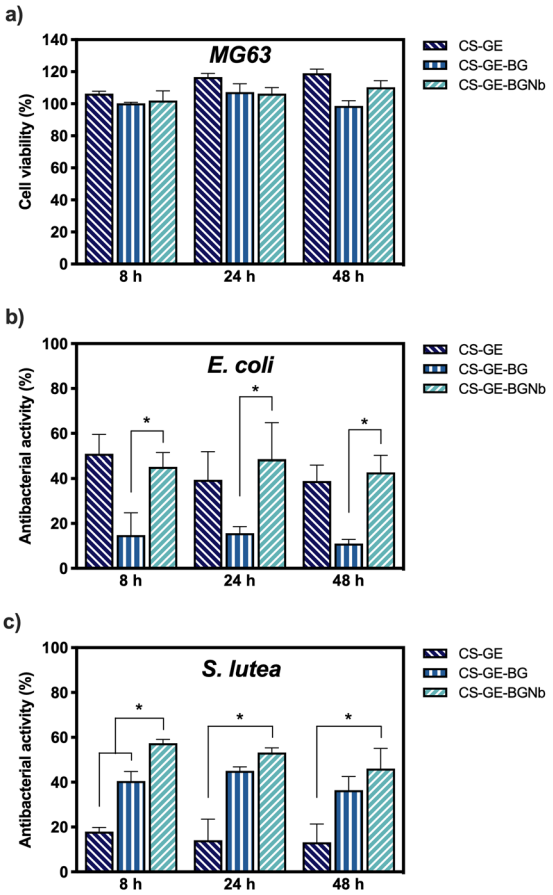

Fig. 5 **a** Indirect cytotoxicity tests of material extracts on MG63 cell line. CS-GE, CS-GE-BG and CS-GE-BGNb samples were incubated with standard culture medium and material extracts (eluates) were collected at 8, 24 and 48 h after incubation. Antibacterial activity of material extracts against **b** Gram negative (*E. coli*) and **c** Gram positive (*S. lutea*) bacterial strains. CS-GE, CS-GE-BG and CS-GE-BGNb samples were incubated with LB and material extracts (eluates) were collected at 8, 24 and 48 h after incubation. Data are expressed as mean ± SD. (*$p < 0.05$)

CS-GE-BG scaffolds inhibited Gram positive bacterial growth of about 40% (Fig. 5c), while displaying a very low antibacterial efficacy (less than 20%) against of *E. coli* (Fig. 5b).

When BG were doped with Nb, the resulting scaffolds displayed improved antibacterial behavior with respect to the CS-GE-BG counterparts, even though to a different extent depending on the bacterial strain tested (antibacterial activity against *E. coli*: ≈50% vs. ≈20%, $p < 0.05$; antibacterial activity against *S. lutea*: ≈60% vs. ≈40%; $p > 0.05$).

It is worthy of note that the greatest antibacterial activity was invariably displayed by the extracts obtained at the shortest incubation time, that was 8 h, suggesting a fast Nb release soon after the incubation of the scaffolds in the extraction medium (Fig. 5; $p > 0.05$: 8 h vs. 24 h vs. 48 h).

4 Discussion

4.1 Manufacturing of chitosan/gelatin/BG scaffolds

Herein, organic/inorganic porous scaffolds for BTE applications were manufactured via EPD. This approach was selected as a rapid yet effective technique to obtain 3D self-standing composite scaffolds, holding several advantages in terms of costs and easy to scale-up process. Uniform scaffolds with microstructural homogeneity and defined porous structure were in fact obtained, based on the original use of CS-GE blends loaded with antibacterial BG.

In this work, the co-deposition of CS-GE-BG for the production, by peeling off, of free-standing scaffolds has been successfully obtained. The presence of GE in the deposited samples was confirmed by the maximum swelling values obtained (see Par. 3.2) for CS-GE samples, in the order of 800%. The obtained swelling values resulted four times higher than those of electrodeposited pure CS samples (SW ≈ 200%), as reported in our previous work [15]. As demonstrated by Abruzzo et al., GE provides a higher water-uptake in CS-GE films, with respect to CS films, for the presence of a great number of ionized amino acids (i.e., free charges) in the GE structure [28].

The electrophoretic co-deposition of CS and GE onto titanium substrate has been reported in previous studies [16]. Since the isoelectric point of gelatin type B (pI = 4.7–5.2 [29]) is lower than the one of chitosan (pI ~ 6.3) GE molecules are less charged at acidic pH, resulting in lower electrophoretic mobility. Therefore we speculate that CS acts as a vehicle to transport GE molecules on the cathode, due to the formation of electrostatic interactions between NH_3^+ groups of CS and COO^- groups GE. The formation of such polyelectrolyte complexes was confirmed, in our work, by the shift of the peak at 1165 cm^{-1}, (stretching vibration of -COOH groups of Glu and Asp in GE), to 1155 cm^{-1} [6, 21].

The presence of BG was assessed both qualitatively, by SEM images, and quantitatively, with TGA analyses. In this regard, it is interesting to notice that the content of BG in the samples, measured by TGA, was comparable to the amount of BG amount loaded (10% w_{BG}/w_{CS+GE}) before the EPD process, demonstrating the efficacy of the technique to allow a fine tune of the scaffold's composition by tuning the electrophoretic bath. It is worthy of notice, however, that this result can be achieved by a correct selection of the processing parameters, including the time between the preparation of the bath and the deposition: long (higher than 30 min) intervals before the use of the bath can results in BG particles settling and composition variations, due to the typical kinetic of reaction of small BG particles [31].

CS-BG co-deposition mechanism was explained by Pishbin et al. [32]. They showed how, below the isoelectric point of BG 45S5 (pI = 11.5), the formation of free hydroxyl groups led to the establishment of hydrogen bonds with chitosan hydroxyl and carbonyl moieties.

4.2 In vitro chemico-physical characterization

Swelling and degradation under physiological conditions must be controlled to avoid the premature resorption and impairment of a bone scaffold [32–34]. Swelling tests on the obtained scaffolds indicate that CS-GE samples possess higher absorption capacity, while showing a faster degradation kinetics when compared to glass-containing specimens. These findings are in accordance with other studies [34, 35], that show how both the swelling rate and degradation rate of BG-containing scaffolds decrease by increasing the total amount of BG. These phenomena can be attributed to the lower hydrophilicity of the inorganic phase compared to the polymer matrix [34]. Moreover, BGs seem to play a significant role in the stability of the CS-GE network, acting as physical crosslinkers: BG particles, interacting through hydrogen bonds and ionic interactions with the polymer molecules, cause a slower relaxation of the polymer chains, thus decreasing the swelling ratio [33, 34]. It is also possible to notice that, for all the samples, the degradation profiles reach a plateau between day 21 and 28 (Fig. 2b). This phenomenon can be associated with the dissolution of the gelatin component in the scaffolds, due to the fact that the test temperature (i.e., T = 37 °C) is higher than the upper critical solution temperature of gelatin (UCST = 32 °C [9]). A similar behavior has been observed in the literature, where by increasing gelatin content into CS-GE scaffolds, an increased degradation rate has been observed [36].

In swelling studies, a rapid increase in the pH of PBS starts immediately after immersion. This pH increase is to be expected, since chitosan is a weakly basic polymer and its degradation leads to the formation of fragments and oligomers that increase the pH of the medium [37]. This phenomenon is combined with the rapid dissolution of glasses, a process which starts with an exchange of Ca^{2+} with H^+ ions from the solution. The ions exchange causes the hydrolysis of the silica groups (Si-O-Si) and the consequent formation of silanol groups (Si-OH), known to be the starting point for HA nucleation [38]. Both the increase in pH and the continuous ion release cause the gradual scaffold dissolution.

The apatite formation ability of the scaffolds has been evaluated via SBF studies up to 28 days. SEM observations, XRD and FT-IR results show a slow (within 21 and 28 days) yet effective nucleation of CaP species on BGs. Previous studies indicate the formation of an apatite layer within 5 and 7 days after soaking CS scaffolds containing the 30% (w/w) of BG [39] and GE scaffolds containing the

20% (w/w) of BG [40]. This delay in the formation of HA deposits can be attributable to the lower amount of BG particles inside our scaffolds (10% w/w). In this regard, it was reported that calcium precipitation occurs only when the soaking solution reaches the ion saturation level [41].

Moreover, as reported by Rezaei et al. [27] the broadness of the XRD diffraction reflects crystal imperfection and lattice strain. According to these considerations, it is possible to state that calcium phosphates formed at day 21 possess a poor crystalline phase. As shown in SEM micrographs (Fig. 3d) and confirmed in FTIR spectra (Fig. 4a), huge calcium phosphate aggregates were identified on CS-GE-BG samples after 28 days of immersion. This deposit appears more crystalline, compared to previous time-points, as confirmed by the sharper peak at $2\theta = 32°$ from XRD analysis (Fig. 4c). Similar considerations can be done for CS-GE-BGNb samples, confirming that Nb did not influence the bioactivity of the scaffolds.

4.3 In vitro biological activity

The properties of the material surface play a crucial role in cell behavior, including adhesion, proliferation, and differentiation. In light of this, in vitro tests provide insight on the cellular response to biomaterials [42]. The use of CS, GE, and BG in BTE is largely reported in literature [6]. Results about cytotoxicity tests performed in this work are in accordance with published data [8, 18], demonstrating that the release of Nb ions in cell culture media have no detrimental effect on cells.

Besides, the antibacterial activity of CS has been widely reported in literature [11, 43] and it has been ascribed to the presence of the positively charged amino groups ($-NH_3^+$) at physiological pH which interact with negatively charged microbial cell membranes. Some evidences demonstrated that CS is more effective against Gram-negative bacteria, being their cell wall more hydrophilic and anionic (negatively charged) than that of Gram-positive bacteria [44]. Accordingly, in this work, eluates from CS-GE scaffolds were found to be much more effective against *E. coli* than *S. lutea* bacteria (Fig. 5). When BG were loaded in CS-GE scaffolds, the antibacterial performances of the resulting materials were different, being CS-GE-BG scaffolds less active against *E. coli* than against *S. lutea*. These findings might be ascribed to the presence of the inorganic phase, i.e., the BG particles, which lower the overall hydrophilicity of the CS-GE-BG scaffolds, thus their interaction with the hydrophilic bacterial walls of *E. coli*.

It has been known that the modification of biomaterials with metal ions, such as Ag^+, Zn^{2+}, Ga^{3+}, allows obtaining materials with significant antimicrobial properties. In this study, we doped CS-GE-BG scaffolds with metal Nb ions by means of ionic substitution and compared the antibacterial effects of such materials against Gram negative (*E. coli*) and Gram positive (*S. lutea*) bacteria with respect to the unmodified counterparts. Interestingly, the addition of Nb-doped CS-GE-BG scaffolds invariably displayed improved antibacterial behavior with respect to the pristine CS-GE-BG scaffolds, even though to a different extent depending on the bacterial strain tested (Fig. 5b—*E. coli*: $p > 0.05$ between CS-GE-BGNb and CS-GE-BG for every extraction time; Fig. 5c—*S. lutea*: $p < 0.05$ between CS-GE-BGNb and CS-GE-BG for every extraction time).

Altogether, these results disclose the CS-GE-BGNb scaffolds as promising biomaterials with inherent antibacterial activity.

5 Conclusions

In this work, we showed a simple yet effective approach to the fabrication of organic-inorganic scaffolds by one-pot electrophoretic deposition procedure. The presence of the inorganic BG component allows the in vitro formation of a mineral phase after 28 days of soaking in SBF solution. The addition of Nb does not affect the formation of a mineral phase (i.e., CaP), confirming the bone-bonding ability of the fabricated scaffolds. Interestingly, CS-GE-BGNb scaffolds exhibit very good antibacterial activity, especially within the first 8 h of test, and the presence of Nb seems to potentiate the antibacterial activity of chitosan. Moreover, cell viability is shown to be unaffected by the presence of Nb, whose release can be considered far from being cytotoxic. With this perspective, CS-GE-BGNb materials are very promising candidates as scaffolds for BTE applications. In this light, further investigations are needed to strengthen our findings and to shed light on CS-GE-BGNb scaffolds influence the cell behavior in vitro.

Acknowledgements Dr Samira Tansaz and Dr Supachai Reakasame (Institute of Biomaterials, University of Erlangen-Nuremberg) are acknowledged for experimental support.

Compliance with ethical standards

Conflict of interest The authors declare that they have no conflict of interest.

References

1. Pina S, Oliveira JM, Reis RL. Natural-based nanocomposites for bone tissue engineering and regenerative medicine: a review. Adv Mater. 2015;27:1143–69.

2. Hoppe A, Güldal NS, Boccaccini AR. A review of the biological response to ionic dissolution products from bioactive glasses and glass-ceramics. Biomaterials. 2011;32:2757–74.
3. Gerhardt L-C, Boccaccini AR. Bioactive glass and glass-ceramic scaffolds for bone tissue engineering. Materials. 2010;3:3867–910.
4. Hoppe A, Mouriño V, Boccaccini AR. Therapeutic inorganic ions in bioactive glasses to enhance bone formation and beyond. Biomater Sci. 2013;1:254–6.
5. El-Kady AM, Ali AF, Rizk RA, Ahmed MM. Synthesis, characterization and microbiological response of silver doped bioactive glass nanoparticles. Ceram Int. 2012;38:177–88.
6. Rehman MAU, Munawar MA, Schubert DW, Boccaccini AR. Electrophoretic deposition of chitosan/gelatin/bioactive glass composite coatings on 316L stainless steel: a design of experiment study. Surf Coatings Technol. 2019;358:976–86. https://doi.org/10.1016/j.surfcoat.2018.12.013.
7. Tamai M, Isama K, Nakaoka R, Tsuchiya T. Synthesis of a novel b-tricalcium phosphate/hydroxyapatite biphasic calcium phosphate containing niobium ions and evaluation of its osteogenic properties. J Artif Organs. 2007;10:22–8.
8. Obata A, Takahashi Y, Miyajima T, Ueda K, Narushima T, Kasuga T. Effects of niobium ions released from calcium phosphate invert glasses containing Nb 2O 5 on osteoblast-like cell functions. ACS Appl Mater Interfaces. 2012;4:5684–90.
9. Campiglio CE, Negrini NC, Farè S, Draghi L. Cross-linking strategies for electrospun gelatin scaffolds Materials 2019;12(15), art. no. 2476. https://doi.org/10.3390/ma12152476.
10. Kong M, Chen XG, Xing K, Park HJ. Antimicrobial properties of chitosan and mode of action: a state of the art review. Int J Food Microbiol. 2010;144:51–63.
11. Vaz JM, Pezzoli D, Chevallier P, Campelo CS, Candiani G, Mantovani D. Antibacterial coatings based on chitosan for pharmaceutical and biomedical applications. Curr Pharm Des. 2018;24:866–85. http://www.eurekaselect.com/159920/article.
12. Avcu E, Baştan FE, Abdullah HZ, Rehman MAU, Avcu YY, Boccaccini AR. Electrophoretic deposition of chitosan-based composite coatings for biomedical applications: a review. Prog Mater Sci. 2019;103:69–108. https://linkinghub.elsevier.com/retrieve/pii/S0079642519300015.
13. Zhang Z, Cheng X, Yao Y, Luo J, Tang Q, Wu H, et al. Electrophoretic deposition of chitosan/gelatin coatings with controlled porous surface topography to enhance initial osteoblast adhesive responses. J Mater Chem B. 2016;4:7584–95.
14. Estrada-Cabrera E, Torres-Ferrer LR, Aztatzi-Aguilar OG, De Vizcaya-Ruiz A, Meraz-Rios MA, Zarate-Triviño DG, et al. Chitosan-bioglass coatings on partially nanostructured anodized Ti-6Al-4V alloy for biomedical applications. Surf Coatings Technol. 2019;375:468–76.
15. Ghalayani EA, Soleimanzade M, Campiglio CE, Federici A, Altomare L, Draghi L, et al. Hierarchical microchannel architecture in chitosan/bioactive glass scaffolds via electrophoretic deposition positive-replica. J Biomed Mater Res Part A. 2019;107:1455–65. https://onlinelibrary.wiley.com/doi/abs/10.1002/jbm.a.36660.
16. Jiang T, Zhang Z, Zhou Y, Liu Y, Wang Z, Tong H. et al. Surface functionalization of titanium with chitosan/gelatin via electrophoretic deposition: characterization and cell behavior. Biomacromolecules. 2010;11:1254–60. https://doi.org/10.1021/bm100050d.
17. Lavenus S, Poxson DJ, Ogievetsky N, Dordick JS, Siegel RW. Stem cell behavior on tailored porous oxide surface coatings. Biomaterials. 2015;55:96–109.
18. Miguez-Pacheco V, de Ligny D, Schmidt J, Detsch R, Boccaccini AR. Development and characterization of niobium-releasing silicate bioactive glasses for tissue engineering applications. J Eur Ceram Soc. 2018;38:871–6. https://linkinghub.elsevier.com/retrieve/pii/S0955221917305149.
19. Bono N, Pennetta C, Sganappa A, Giupponi E, Sansone F, Volonterio A, et al. Design and synthesis of biologically active cationic amphiphiles built on the calix[4]arene scaffold. Int J Pharm. 2018;549:436–45. https://linkinghub.elsevier.com/retrieve/pii/S0378517318305969.
20. Fernandes Queiroz M, Melo K, Sabry D, Sassaki G, Rocha H. Does the use of chitosan contribute to oxalate kidney stone formation. Mar Drugs. 2014;13:141–58. http://www.mdpi.com/1660-3397/13/1/141.
21. Voron'ko NG, Derkach SR, Kuchina YA, Sokolan NI. The chitosan–gelatin (bio)polyelectrolyte complexes formation in an acidic medium. Carbohydr Polym. 2016;138:265–72. https://linkinghub.elsevier.com/retrieve/pii/S0144861715011492.
22. Ochoa I, Sanz-Herrera JA, García-Aznar JM, Doblaré M, Yunos DM, Boccaccini AR. Permeability evaluation of 45S5 Bioglass®-based scaffolds for bone tissue engineering. J Biomech. 2009;42:257–60. https://linkinghub.elsevier.com/retrieve/pii/S0021929008005563.
23. Matos MC, Ilharco LM, Almeida RM. The evolution of TEOS to silica gel and glass by vibrational spectroscopy. J Non Cryst Solids. 1992;147–148:232–7. https://linkinghub.elsevier.com/retrieve/pii/S0022309305806222.
24. Flambard A, Videau JJ, Delevoye L, Cardinal T, Labrugère C, Rivero CA, et al. Structure and nonlinear optical properties of sodium–niobium phosphate glasses. J Non Cryst Solids. 2008;354:3540–7. https://linkinghub.elsevier.com/retrieve/pii/S0022309308001658.
25. ElBatal H, Azooz M, Khalil EM, Soltan Monem A, Hamdy Y. Characterization of some bioglass–ceramics. Mater Chem Phys. 2003;80:599–609. https://linkinghub.elsevier.com/retrieve/pii/S0254058403000828.
26. Pishbin F, Mouriño V, Flor S, Kreppel S, Salih V, Ryan MP. et al. Electrophoretic deposition of gentamicin-loaded bioactive glass/chitosan composite coatings for orthopaedic implants. ACS Appl Mater Interfaces. 2014;6:8796–806. https://doi.org/10.1021/am5014166.
27. Rezaei Y, Moztarzadeh F, Shahabi S, Tahriri M. Synthesis, characterization, and in vitro bioactivity of sol-gel-derived SiO 2 –CaO–P 2 O 5 –MgO-SrO bioactive glass. Synth React Inorg, Met Nano-Metal Chem. 2014;44:692–701. https://doi.org/10.1080/15533174.2013.783869.
28. Abruzzo A, Bigucci F, Cerchiara T, Cruciani F, Vitali B, Luppi B. Mucoadhesive chitosan/gelatin films for buccal delivery of propranolol hydrochloride. Carbohydr Polym. 2012;87:581–8. https://linkinghub.elsevier.com/retrieve/pii/S014486171100703X.
29. Aramwit P, Jaichawa N, Ratanavaraporn J, Srichana T. A comparative study of type A and type B gelatin nanoparticles as the controlled release carriers for different model compounds. Mater Express. 2015;5:241–8. https://doi.org/10.1166/mex.2015.1233.
30. Popat A, Liu J, Lu J, Qiao GQ (Max), Zhang S. A pH-responsive drug delivery system based on chitosan coated mesoporous silica nanoparticles. J Mater Chem. 2012;22:11173. http://xlink.rsc.org/?DOI=c2jm30501a.
31. Cerrutti M, Greenspan D, Powers K. An analytical model for the dissolution of different particle size samples of Bioglass in TRIS-buffered solution. Biomaterials. 2005;26:4903–11. https://linkinghub.elsevier.com/retrieve/pii/S0142961205000384.
32. Pishbin F, Simchi A, Ryan MP, Boccaccini AR. A study of the electrophoretic deposition of Bioglass® suspensions using the Taguchi experimental design approach. J Eur Ceram Soc. 2010;30:2963–70. https://linkinghub.elsevier.com/retrieve/pii/S0955221910001329.
33. Maji K, Dasgupta S, Pramanik K, Bissoyi A. Preparation and evaluation of gelatin-chitosan-nanobioglass 3D porous scaffold

for bone tissue engineering. Int J Biomater. 2016;2016:1–14. http://www.hindawi.com/journals/ijbm/2016/9825659/.
34. Gentile P, Mattioli-Belmonte M, Chiono V, Ferretti C, Baino F, Tonda-Turo C. et al. Bioactive glass/polymer composite scaffolds mimicking bone tissue. J Biomed Mater Res Part A. 2012;100A:2654–67. https://doi.org/10.1002/jbm.a.34205.
35. Peter M, Binulal NS, Nair SV, Selvamurugan N, Tamura H, Jayakumar R. Novel biodegradable chitosan–gelatin/nano-bioactive glass ceramic composite scaffolds for alveolar bone tissue engineering. Chem Eng J. 2010;158:353–61. https://linkinghub.elsevier.com/retrieve/pii/S1385894710000963.
36. Han F, Dong Y, Su Z, Yin R, Song A, Li S. Preparation, characteristics and assessment of a novel gelatin–chitosan sponge scaffold as skin tissue engineering material. Int J Pharm. 2014;476:124–33. https://linkinghub.elsevier.com/retrieve/pii/S0378517314006917.
37. Wan Y, Wu H, Cao X, Dalai S. Compressive mechanical properties and biodegradability of porous poly(caprolactone)/chitosan scaffolds. Polym Degrad Stab. 2008;93:1736–41. https://linkinghub.elsevier.com/retrieve/pii/S0141391008002607.
38. Hench LL. Bioceramics: from concept to clinic. J Am Ceram Soc. 1991;74:1487–510. https://doi.org/10.1111/j.1151-2916.1991.tb07132.x.
39. Mota J, Yu N, Caridade SG, Luz GM, Gomes ME, Reis RL, et al. Chitosan/bioactive glass nanoparticle composite membranes for periodontal regeneration. Acta Biomater. 2012;8:4173–80. https://linkinghub.elsevier.com/retrieve/pii/S1742706112002978.
40. Nadeem D, Kiamehr M, Yang X, Su B. Fabrication and in vitro evaluation of a sponge-like bioactive-glass/gelatin composite scaffold for bone tissue engineering. Mater Sci Eng C. 2013;33:2669–78. https://linkinghub.elsevier.com/retrieve/pii/S0928493113001215.
41. Pereira MM, Clark AE, Hench LL. Calcium phosphate formation on sol-gel-derived bioactive glassesin vitro. J Biomed Mater Res. 1994;28:693–8. https://doi.org/10.1002/jbm.820280606.
42. Shin H, Jo S, Mikos AG. Biomimetic materials for tissue engineering. Biomaterials. 2003;24:4353–64. https://linkinghub.elsevier.com/retrieve/pii/S0142961203003399.
43. Cheung R, Ng T, Wong J, Chan W. Chitosan: an update on potential biomedical and pharmaceutical applications. Mar Drugs. 2015;13:5156–86. http://www.mdpi.com/1660-3397/13/8/5156.
44. Silhavy TJ, Kahne D, Walker S. The bacterial cell envelope. Cold Spring Harb Perspect Biol. 2010;2:a000414–a000414. https://doi.org/10.1101/cshperspect.a000414.